Nuclear Instruments and Methods in Physics Research A 346 (1994) 196–204
North-Holland

NUCLEAR INSTRUMENTS & METHODS IN PHYSICS RESEARCH Section A

Development of a new SARA/IGISOL technique for the study of short-lived products from heavy-ion-induced fusion–evaporation reactions

R. Béraud [a], A. Emsallem [a], A. Astier [a], R. Bouvier [a], R. Duffait [a], Y. Le Coz [a], S. Morier [a], A. Wojtasiewicz [a,1], Yu.A. Lazarev [b], I.V. Shirokovsky [b], I.N. Izosimov [b,2], D. Barnéoud [c], J. Genevey [c], A. Gizon [c], R. Guglielmini [c], G. Margotton [c], J.L. Vieux-Rochaz [c]

[a] *Institut de Physique Nucléaire de Lyon, IN2P3-CNRS et Université Claude Bernard 43, Bd du 11 Novembre 1918, 69622 Villeurbanne Cedex, France*

[b] *Joint Institute for Nuclear Research, 141980 Dubna, Russian Federation*

[c] *Institut des Sciences Nucléaires de Grenoble, 53, IN2P3-CNRS et Université Joseph Fourier, Avenue des Martyrs, 38026 Grenoble Cedex, France*

(Received 3 March 1994)

A new ion guide chamber has been designed for heavy-ion (HI) induced fusion–evaporation reactions. Its principle is based on the beam projectiles-evaporation residues separation which is achieved by taking advantage of their very different angular distributions after passing a thick target. In this work it is proved that the IGISOL technique can be applied with an overall efficiency $> 10^{-3}$ for the study of mass-separated exotic nuclei produced in (HI, xn) reactions.

1. Introduction

The study, after on-line mass separation, of nuclei far off the β-stability valley is one of the most fruitful approaches to a better understanding of nuclear structure. Since we have to deal with short-living radioactive beams, the development of fast and sensitive techniques is of utmost importance. The ion-guide based on-line mass separation (IGISOL) initially developed by Ärje et al. [1] is one of them and it led, during the last decade, to the discovery of a large number of new isotopes. In the IGISOL technique, the reaction products recoiling out of a thin target are thermalized in helium gas, extracted as 1^+ ions, and injected in the acceleration stage of the separator. Provided the survival time of the 1^+ charge state is of the same order as the evacuation time, mass separation of the products can be performed with an efficiency of a few percent for all elements. In case of light-ion-induced fusion reactions, this has been achieved even for nuclei with half-lives in the ms range.

The use of IGISOL in heavy-ion (HI) induced fusion–evaporation reactions was rather limited till now because of the so-called "plasma effect" [2]. The HI beam creates in the helium pressurized chamber a dense plasma so that most of the products thermalized as 1^+ ions are neutralized before being evacuated. It has been shown that under such conditions the overall efficiency is considerably reduced because only a small volume near the exit hole is evacuated in time [3]. The plasma effect can be avoided if we separate reaction products from beam particles and let only the products enter the He gas stopping chamber. This was successfully achieved in the case of fission reaction by means of a double chamber designed by Taskinen et al. [4]. For HI induced reactions, in which the recoil products are forward peaked, the same arrangement cannot be applied. At RIKEN the HI beam suppression has been achieved by setting the IGISOL chamber at the focal plane of a high efficiency gas-filled recoil separator (GARIS) [5]. With this GARIS/IGISOL system, overall efficiencies of the order of 0.15% have been reported so far for (^{40}Ar, xn) fusion reactions [6].

An alternative is the "shadow" method which takes advantage of the huge difference of the primary beam angular distribution and that of the reaction products after passing a thick target (about a few mg/cm^2). It was successfully applied by Sprouse et al. [7] for laser spectroscopy experiments. In this paper, the basic principles of the shadow method will be given and our new SARA/IGISOL chamber described in detail. The overall efficiency in $\sim$ 5-MeV/u ^{40}Ar and ^{40}Ca induced fusion–evaporation reactions has been measured and the first results on the mass identification and study of very neutron-deficient nuclei will be presented.

[1] On leave from Institute of Experimental Physics, Warsaw University, 69 Hoza Street, PL-00-681 Warsaw, Poland.

[2] V.G. Khlopin Radium Institute, 197022 Saint Petersburg, Russian Federation.

SSDI 0168-9002(94)00351-7

2. Instrumentation

2.1. Basic principles

It is well known that evaporation residues (EVRs) from HI-induced fusion–evaporation reactions are emitted in a cone centered (along the beam direction) around 0° angle. The angular width of this cone is caused by the three main physical effects.

i) Finite angular spread of the projectile beam, which is determined by the accelerator and its beam optics.

ii) Kinematic effects arising from particle evaporation after fusion. Assuming isotropic particle emission in the center-of-mass (c.m.) system, a number of calculations have been performed to account for kinematic properties [8,9] of EVRs from heavy-ion induced Compound-Nucleus (CN) reactions. An approximate formula for the mean scattering angle $\bar{\alpha}$ in the laboratory system has been derived in ref. [9],

$$\bar{\alpha}(\mathrm{rad}) = 0.39 A_c/(A_c - 1)\left[n\tilde{E}_n/A_p E_p\right]^{1/2},$$

where n is the number of evaporated neutrons with mean energy $\tilde{E}_n$ in the c.m. system, A_c is the mass number of the CN, A_p is that of the beam projectiles, and E_p is the laboratory bombarding energy expressed in MeV. This angle is determined mainly by the $A_p E_p$ factor and it is independent of the target thickness.

iii) The scattering of EVRs in the target may be treated in a classical approach since $Z_p Z_t/137\beta \gg 1$ for both beam particles and recoil products. The mean angular deflection at half-height of the scattered particle distributions $\tilde{\alpha}_{1/2}$ is given by the following approximate expression

$$\tilde{\alpha}_{1/2}(\mathrm{deg}) \simeq \frac{Z_p Z_t}{E_p} \frac{1}{\sqrt{A_t}} \sqrt{\rho \Delta x},$$

where Z_t and A_t are charge and mass numbers of the target, respectively, and $\rho\Delta x$ is the target thickness in g/cm^2.

The difference between the angular distribution of projectiles and that of EVRs is mainly due to multiple scattering in the target, whereas beam divergence and particle evaporation are of minor importance. It has been shown in ref. [10] that the ratio of the angular half-widths α_p/α_c for beam projectiles and EVRs after crossing the same target can be approximated as

$$\frac{\alpha_p}{\alpha_c} \simeq \frac{Z_p}{Z_c} \frac{A_p}{A_c}.$$

As an example, let us consider two projectile–target combinations, the ^{40}Ca + ^{144}Sm reaction and the ^{90}Zr + ^{94}Mo one, which lead to the same ^{180}Pb nucleus via the 4n-evaporation channel. The preceding formula indicates that EVRs are diffused in a larger solid angle for the lighter beam projectiles. Therefore a better separation is expected to be achieved with the lighter projectiles.

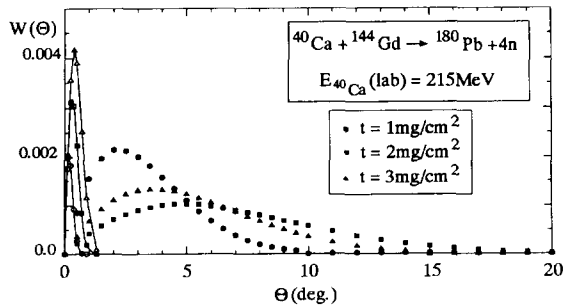

Fig. 1. Angular distributions $W(\theta) = [\mathrm{d}\sigma(\theta)/\mathrm{d}\theta]/\sigma$ of the ^{180}Pb EVRs (closed symbols) as calculated by Sagaidak [12] for different target thicknesses t. The multiple scattering of the 215-MeV ^{40}Ca beam (open symbols) in the target is also shown for comparison.

At the beginning of this work, one of our physics goals was the alpha- and beta-decay study of the nucleus ^{180}Tl ($T_{1/2} \simeq 1$ s) tentatively assigned by Lazarev et al. [11]. This isotope which undergoes EC-delayed fission was produced via the ^{144}Sm(^{40}Ca, p3n) reaction. Therefore the first simulation has been carried out for this beam–target combination. Assuming similar angular distributions for the p3n- and 4n-channels, a calculation was performed by Sagaidak [12] for the ^{40}Ca + ^{144}Sm → ^{180}Pb + 4n reaction at 215 MeV bombarding energy. The results presented in Fig. 1 show that for target thicknesses between 1 and 3 mg/cm^2 the primary beam is confined within a 1° angle whereas the reaction products are spread over a 15° angle. In principle, a simple geometrical arrangement (like a beam stop or a beam channel described in section 2.2) is able to suppress more than 99% of the primary beam while allowing more than 50% of the EVRs to penetrate in the thermalization chamber.

This kinematic effect provides us with a simple method to prevent the primary beam from interacting with the buffer gas. A beam stop can be placed between the target and the thermalization chamber [7]. In our case a metallic tube is employed to conduct the beam through the chamber without interacting with helium.

2.2. The new IGISOL chamber

2.2.1. Description

Fig. 2 shows a layout of the new chamber of the IGISOL facility installed on-line with SARA in Grenoble. The cylindrical metallic tube ($\phi_i = 6$ mm) conducts $\simeq 99\%$ of the beam intensity to a beam catcher (not presented in Fig. 2) where the energy of the beam can be easily dissipated and its intensity measured. This system was designed to exploit the beam–EVR separation under various kinematic conditions. In particular, the target-to-

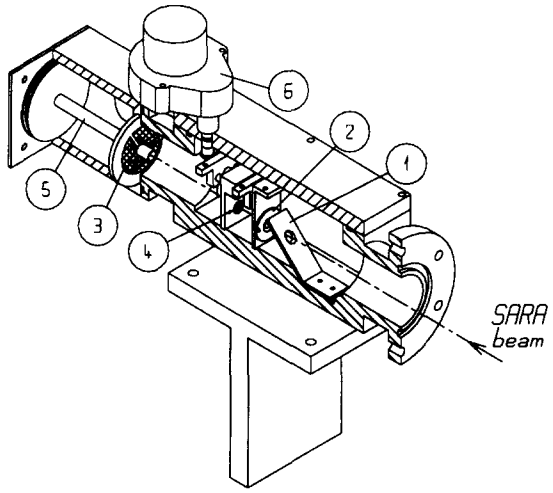

Fig. 2. The cut-away view shows the ZnS diaphragm (1) used to focus the cyclotron beam on the target, the carbon diaphragm (2) which defines the beam position, the entrance window (3) ($\phi_e = 30$ mm, $\phi_i = 10$ mm, effective area ~ 570 mm^2), the target holder (4), as well as the cylindrical thermalization chamber ($\phi = 5$ cm, $l = 6$ cm) of ~ 115 cm^3 surrounding the beam suppression tube (5), target positioning motor (6).

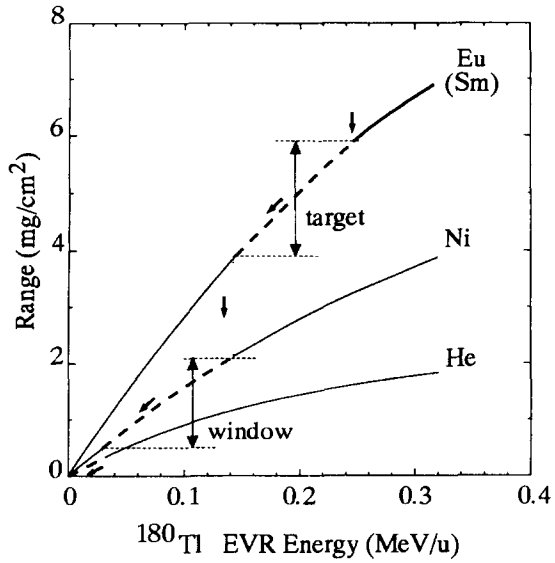

Fig. 3. Range–energy curves for different materials in a foil stack (Eu–Ni–He) extracted from ref. [13]. The dashed line indicates the progression of energy loss of 2.5-MeV/u Tl products. It has been considered that ranges of EVRs in Sm (target) and Eu were identical

window distance can be varied from 9 to 11 cm by using a remote-controlled motor.

2.2.2. Range calculations and stopping of the products

In HI-induced fusion–evaporation reactions, the EVRs acquire a large recoil energy so that their thermalizing in a gas is a major problem. If we assume isotropic particle emission in the c.m. system, the recoil energy E_R is related to the bombarding energy E_B by the following equation

$$E_R = \frac{m_R m_B}{(m_B + m_T)^2} E_B,$$

where m_B, m_T, m_R are masses of the projectile, the target, and the residue, respectively. Some typical E_R values are given in Table 1 for various reactions of interest, showing that the average EVR energy E_R is ranging from 45 to 62 MeV.

Using Northcliffe and Shilling tables [13], it is possible to get a rough estimate of the stopping efficiency of our chamber. This is illustrated in Fig. 3 for the ^{144}Sm + ^{40}Ca reaction. The EVRs produced at the entrance of the 2-mg/cm^2 ^{144}Sm target with the recoil energy $E_R = 0.25$ MeV/u are slowed down in the target to ~ 0.14 MeV/u and then pass the 1.7-mg/cm^2 Ni window before entering the He gas chamber with an energy of ~ 0.02 MeV/u corresponding to a range in helium of ~ 0.3 mg/cm^2, whereas the EVRs produced at the exit of the target have a ~ 0.9 mg/cm^2 range. The length of the thermalization chamber (6 cm) has been chosen in a way to allow us to optimize the number of EVRs stopped in He (taking into account that the He pressure compatible with the pumping speed of our vacuum system is $\simeq 500$ mbar) and also to keep the mean evacuation time at a reasonable value. The conductance is estimated by the relation $C(\mathrm{l/s}) = 0.45\ \phi_e^2$ (mm). Hence, for a 1.2-mm diameter extraction hole, the mean evacuation time of the 115-cm^3 chamber is about 180 ms.

A simulation performed with the TRIM code [14] makes it possible to choose an appropriate Ni window thickness (1.7 mg/cm^2 in this case) in order to optimize the number of EVRs thermalized in He. About 30–75% of EVRs are stopped with the He pressure ranging from 300 to 600 mbar.

Table 1
Beam and target combinations used in our experiments

Isotope	Beam	Target	Beam energy (MeV)	E_R (MeV)
^{180}Tl	^{40}Ca	^{144}Sm	215	45
^{150}Dy	^{40}Ar	^{116}Cd	190	47
^{132}Nd	^{40}Ca	^{96}Mo	210	60

2.3. Connection with the isotope separator

After passing the Ni entrance window, EVRs are thermalized in He, then transferred as singly charged ions by the flow through the $\phi = 1.2$ mm exit aperture guided to the $\phi = 2$ mm skimmer, and then accelerated towards the

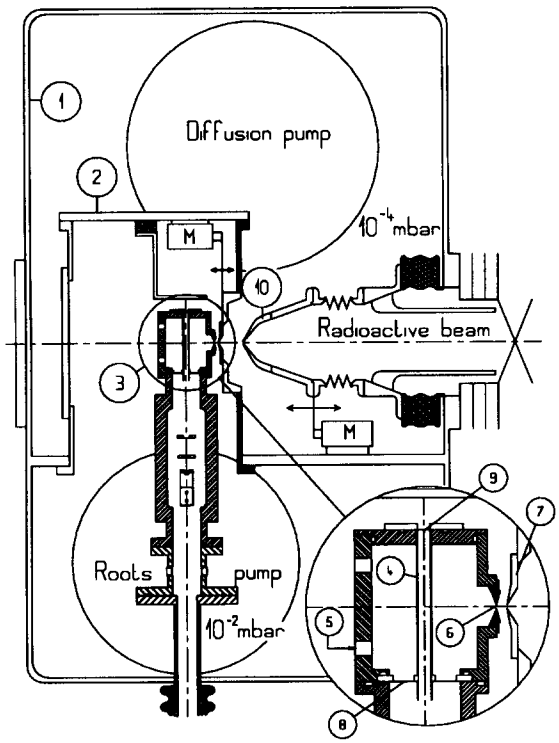

Fig. 4. Schematic top view of the new SARA IGISOL system designed for HI-induced fusion–evaporation reactions. general purpose vacuum chamber (1), inner chamber (2) the insert (3) shows the beam suppression tube (4), the He inlet (5), the $\phi = 1.2$ mm extraction hole (6), the $\phi = 2$ mm skimmer (7), the $\phi = 30$ mm entrance window (8), and the beam exit window (9). The acceleration electrode (10) with $\phi = 5$ mm shown with its stainless steel bellows is connected to the ground potential.

separation magnet. This part of the set-up as well as the pumping system and control devices have been described in detail in our previous paper [15] related with the ^{238}U (40-MeV α, fission) reaction. Fig. 4 shows a top view of the new set-up.

The tuning of the IGISOL optics was performed with stable $^{128-136}Xe^{+}$ ions produced by the scattered primary beam on a small amount of Xe gas mixed with He gas. The mass resolving power $M/\Delta M$ was typically ~ 300 at a He pressure of 500 mbar and an acceleration voltage of 25 kV.

3. Experimental

3.1. Yield as a function of He pressure

In the case of HI-induced fusion–evaporation reactions it is of prime importance to increase the stopping power of the chamber because of the large velocities of the recoil products. This can be done by increasing the He pressure, provided an efficient differential pumping system allows the vacuum in the acceleration stage of the mass separator to be kept below typically a few 10^{-4} mbar.

In order to adjust all parameters for the highest separation efficiency, it is desirable, first, to choose a reaction with a large cross-section and, second, to have a high detection sensitivity. In this study the prolific ^{116}Cd(^{40}Ar, 6n)^{150}Dy reaction has been chosen. Fig. 5 shows the yield of the α-emitter ^{150}Dy ($T_{1/2} = 7.2$ min) as a function of He pressure. The extracted yield increases almost linearly with increasing the He pressure up to 500 mbar. A similar result was obtained with the GARIS/IGISOL system [6] which is completely free of primary beam in the thermalization chamber.

The mass resolving power ($M/\Delta M$) is smoothly decreasing from ~ 500 to ~ 350 when the He pressure increases from 250 to 500 mbar. At higher pressure values, the mass resolution is limited mainly by the energy spread due to collisions in the relatively high-pressure helium between the extraction hole and the skimmer electrode. Because of line broadening, both the yield and the mass resolving power are strongly reduced. To overcome this difficulty, it was suggested to introduce an electric dipole in order to achieve energy dispersion compensation [16] based on velocity focussing, or to use a "squeezer" ion guide [17] which makes it possible to bring ions with low kinetic energy (typically 10 eV) into a high vacuum for further acceleration.

From the range-energy curves displayed in Fig. 6, it can be seen that ^{150}Dy EVRs produced at the entrance of the target, after slowing down in both the 2-mg/cm^2 ^{116}Cd target and 1.7-mg/cm^2 Ni window, have still a minimum range of about 0.2 mg/cm^2 in helium. This is in good

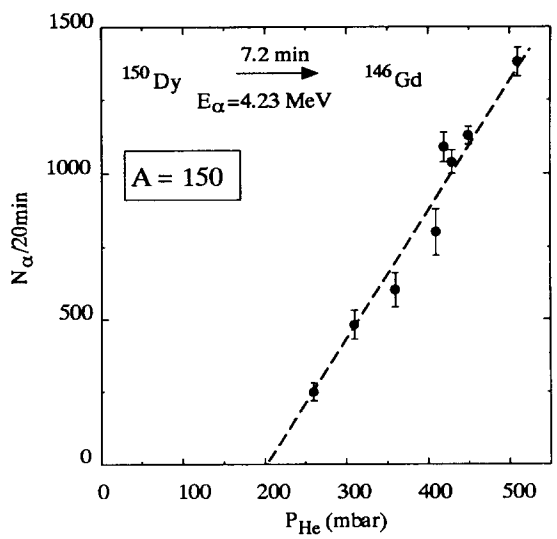

Fig. 5. Yield of ^{150}Dy as a function of He pressure. The uncertainty in pressure is about ±10 mbar. The dashed line is to guide the eye. The $^{40}Ar^{11+}$ beam intensity was fixed at 30 pnA.

agreement with the extrapolation of the dashed line shown in Fig. 5 since the length of our chamber is 6 cm. Considering the maximum range of the products (~ 1 mg/cm^2 in helium), it can be estimated that with this target and window configuration at most 30% of them are stopped at 500 mbar. The remainder is implanted in the walls and is therefore lost for mass separation.

It is worth noting that the extracted yield could be increased with similar pressure provided a better matching is achieved between reaction kinematics and stopping powers of target, window and He pressurized chamber. More precisely, by increasing the thickness of the entrance window, the curve of Fig. 5 can be shifted to the left thus increasing the fraction of the EVRs stopped in He.

In a simple picture of ambipolar diffusion of ions in He at room temperature and pressure P (mbar), one can get an average value for the diffusion coefficient (D_a in cm^2/s) via the equation given by Biondi and Brown [18]: $D_a = 650/P$.

By solving the diffusion equation of ions inside a cylinder, we may estimate the time τ(s) necessary for the 1/e fraction of the ions to diffuse over a mean distance X (cm) from the following relationship:

$$\tau(\mathrm{s}) = \frac{1}{D_a}\left(\frac{X}{2.4}\right)^2 .$$

For an ion thermalized at a pressure of 500 mbar and at a distance of 10 mm from the walls of the chamber or channel, the mean diffusion time is about 130 ms according to the above equations. If we assume a homogeneous evacuation of the chamber (mean evacuation time ~ 180 ms), it is obvious that working at a higher pressure will reduce diffusion losses.

The most remarkable result is the fact that with increasing the helium pressure in our chamber the losses due to the recombination with electrons created by the non-suppressed part of the primary beam are of minor importance compared to the stopping efficiency increase.

3.2. Overall efficiency of the IGISOL system

To determine the absolute average efficiency of our IGISOL system we have been using nuclear reactions with large cross sections producing well-known radioactive products. This is particularly the case for the α-emitter ^{150}Dy produced by ^{116}Cd(^{40}Ar, 6n). The bombarding energy was fixed at 190 MeV at the entrance of a 2-mg/cm^2 thick ^{116}Cd target (enriched to 93.3%) in order to optimize the production rate according to ref. [19]. Using a 500-μm thick surface-barrier Si detector, we measured the 4.233-MeV α-ray intensity in well defined geometries in two separate experiments

i) first, after on-line mass separation and collection on a tape drive for on-line counting;

ii) secondly, the recoiling reaction products were collected on an Al catcher foil placed on the $\phi = 30$ mm entrance window of the IGISOL recoil chamber and were counted off line.

The absolute efficiency ϵ obtained from the ratio of the two above yields has, after solid-angle and decay corrections, the following value: $\epsilon = (1.4 \pm 0.3) \times 10^{-3}$ at $p_{He} = 420$ mbar. It is worth noting that the efficiency is strongly pressure dependent (see section 3.1 and Fig. 5).

3.3. Ionization and recombination processes

In a first approximation it can be considered that EVRs are thermalized as 1^+ ions. This may be explained simply by the value of the ionization potential of He (24.6 eV) which is much larger than that for all other elements (5–10 eV) except for Ne (21.6 eV). Furthermore, the second ionization potential for most of the elements is close to 20 eV. During the thermalization EVRs can exchange charges (e^-) with the He atoms until they arrive to the 1^+ charge state. Then, the EVRs cannot be neutralized anymore by capturing electrons from He and they may survive a rather long time in pure He gas. Of course this picture is oversimplified and additional effects can limit the survival time of these 1^+ ions to a few milliseconds. Some of these effects limiting the efficiency of the IGISOL technique have been identified. In this paragraph we describe our studies on the two important second-order effects: i) the effect of impurities contained in the He gas; and ii) the effect of thermalized electrons in the He gas. We call them the second-order effects because after the first step of the process leading to a 1^+ ion these give some ideas of the de-ionization and can indicate the parameters on which we should work in order to optimize the efficiency of the system.

3.3.1. The impurity effect

The impurities contained in He have a low ionization potential and thus can be easily ionized by exchanging e^- with 1^+ EVRs. This results in a drastic reduction of the efficiency even if the impurities are in microscopic quantity. In order to minimize this effect we have to use ultra-pure He gas and it is necessary to purify it again by passing the gas through a cryogenic trap. Moreover, a certain duration of the degasing phase is needed before steady conditions are obtained. In a test experiment, we measured the yield of ^{150}Dy. A "good" vacuum is obtained after one or two hours of pumping, however at this time a large amount of molecular ions produced by the ionization of oxygen, nitrogen and water molecules are still detected at the end of the apparatus, whereas low yield is obtained for the EVRs. In several hours the production of molecular ions decreases and the EVRs yield increases. A degasing period from 6 to 12 hours is needed to get a stable extraction and detection rate.

3.3.2. The plasma effect

Neutralization of the 1^+ ions can occur inside the recoil chamber by recombination of the 1^+ ions with free electrons present in the He gas. These e^- are produced in large amounts from interactions of beam particles with the He atoms, from the thermalization process of EVRs, as well as from secondary electrons emitted by the windows of the chamber. This "plasma effect" was believed to be the main limitation to the efficiency obtained with the IGISOL method. A first estimate of this effect was performed by Morita et al. [2] who studied the yield of their IGISOL system as a function of the energy ΔE deposited per second by the beam in the He gas. A rapid decrease in the yield was observed with ΔE larger than 10^{16} eV/s. This effect would be a drastic limitation of the application of the IGISOL technique for HI-induced fusion–evaporation reactions since the energy deposited in 500 mbar He, e.g., by 150 enA $^{40}Ar^{11+}$ beam is several times 10^{18}eV.

In our experiments, the strength of the plasma effect was tested in the following way. The yield of mass separated ^{150}Dy was measured with and without the beam-channeling tube, for different beam intensities and different He pressure values. Fig. 7 presents the yield of ^{150}Dy from a series of 600-s measurements performed at beam intensities ranging between 50 and 600 enA.

This figure shows clearly a rather constant yield for an energy deposit ΔE ranging from 2×10^{15} to 2×10^{17} eV/s and then a slow decrease. The beam suppression system allows us to get the better yield. It is worth noting that this result is not in agreement with what was known about the plasma effect. Without the beam suppression, the maximum energy deposited by the ^{40}Ar beam is ΔE

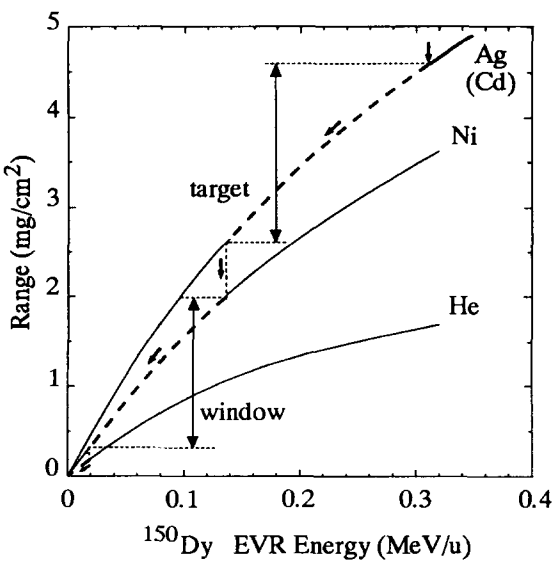

Fig. 6. Range–energy curves for the Cd–Ni–He foil stack used in the pressure dependence study. The dashed line indicates the progression of energy loss of 0.31-MeV/u ^{150}Dy products.

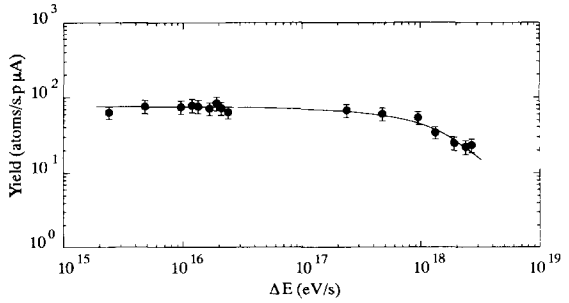

Fig. 7. Yield of ^{150}Dy measured at p_{He} = 420 mbar as a function energy deposited in the IGISOL chamber. The group of points on the left part of the figure has been obtained with the beam-channeling tube by taking into account the measured efficiency of channeling (99%) whereas the right-hand points were obtained without the beam-channeling tube.

$\simeq 3\times10^{18}$ eV/s in our case, which is an order of magnitude larger compared with the range explored in ref. [2]. With such a large energy deposit, one could expect from ref. [2] a vanishingly small yield, which obviously is not the case. This indicates that our representation of the "plasma effect" was oversimplified. For interpreting this result we have to consider that:

i) the plasma effect can be limited to a fraction of the thermalization volume around the particle beam;

ii) the recoil nuclei, scattered beam particles, and secondary electrons produce a dense plasma ($n_e^-/n_{He} \sim 10^{-5}$) which is composed of an equal number of negatively and positively charged He^+ particles needed to keep the electrical balance. The neutralization induced by the plasma electrons may compete with the reionization of EVRs produced by interaction with He^+ ions. The results on Fig. 7 showing a decrease of the yield by only a factor ~ 3 when the plasma density is increasing by two orders of magnitude support the reality of this complex multistep ionization process.

These two processes result in a multistep recombination-reionization mechanism, already mentioned by Ärje [20]. This "second-order" plasma effect does not lead to complete neutralization as it was expected before, but only to a reduction of the yield. An EVR thermalized far off the exit hole will probably undergo neutralization and reionization several times before being extracted as an 1^+ ion.

3.3.3. The mean delay time

In previous sections we have presented results that could be deduced from overall yield measurements. It is also of importance to extract information on the survival time and the evacuation time of 1^+ ions. Provided the lifetime of the radioactive species is long enough, the interplay of these two times will mainly determine the fraction of EVRs extracted as 1^+ ions.

Assuming a laminar gas flow, the mean evacuation time is $\sim$ 180 ms for our chamber (V = 115 cm^3, ϕ_ϵ = 1.2

mm). Of course this estimation is not relevant to the real physical situation because the actual time distribution is broad due to the various distances (0–3 cm) between the exit hole and thermalization sites. This point will be addressed later.

The measurement of the delay time was achieved by using two beam profilers, described in ref. [15], the signals from which were monitored with a digital memory oscilloscope. Stable Xe gas injected in the chamber was ionized by reaction products and by the scattered Ar beam of the accelerator which was pulsed. The time cycle used for this experiment had a 100-ms beam-on and a 100-ms beam-off period. The first beam profiler measuring the $^{40}Ar^{+}$ beam signal was located 1 meter ahead of the ion guide, whereas the second one measuring signal of the mass-separated $^{129}Xe^{+}$ ion was installed at the focal plane of the separator magnet. An example of registered signals is displayed in Fig. 8. Their exponential behaviour is related to the integration time of the electronics and therefore has no physical meaning, whereas the delay between the two signals may be considered as a rather good evaluation of the mean delay time since the oscilloscope was triggered by the generator giving the beam pulsation.

With a 25-kV acceleration voltage, the $\simeq$ 1-μs time of flight of $^{129}Xe^{+}$ ions along the 4 m path (from the ion guide to the focal plane) can be neglected and thus it is possible to study the mean delay time as a function of He pressure. The result of this experiment presented in Fig. 9 exhibits an unexpected dependence of the mean delay time varying from $\sim$ 10 ms to 5 ms when the pressure increases from 100 to 500 mbar. When comparing these values to the mean evacuation time ($\sim$ 180 ms) it can be concluded that only 3–6% of the total amount of $^{129}Xe^{+}$ ions produced in the chamber can be extracted before neutralization. As was already stated by Deneffe et al. [3], only a small fraction ($\simeq$ 5.5% at P_{He} = 100 mbar and $\simeq$ 2.8% at P_{He} = 500 mbar) of the thermalization volume is effective. However, in the real operation conditions the ionization efficiency may be in fact much higher because the intensity of Xe^{+} ions was measured during the beam-off time, without reionization.

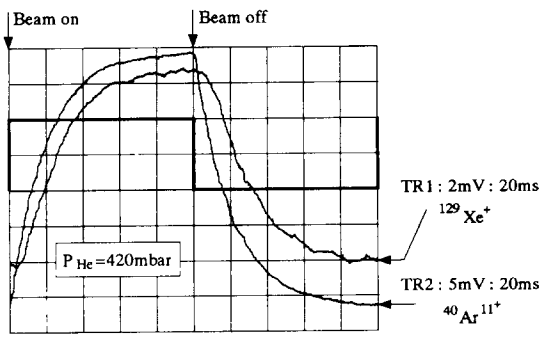

Fig. 8. $^{40}Ar^{11+}$ and $^{129}Xe^{+}$ ion signals measured with a digital memory oscilloscope. The square signal represents the pulsation generator signal with $T_{on} = T_{off}$ = 100 ms.

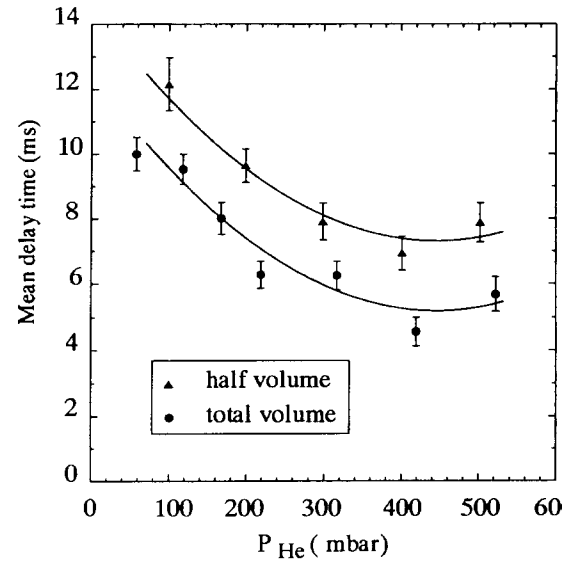

Fig. 9. Mean delay time between Ar and Xe beams as a function of He pressure with $\dot{I}(^{40}Ar^{11+})$ = 250 enA.

In order to check this assumption, a similar experiment was carried out using a semicircular Al beam stop (ϕ = 30 mm) fixed on the entrance havar window for preventing the ^{40}Ar beam particles or recoil products from entering the half volume located close to the exit hole. From Fig. 9 it is clearly seen that the mean delay time is now $\sim$ 3 ms longer than the value measured previously for the total volume.

By comparing the yield in both conditions it is also possible to derive that only 16% of the ions may survive more than 3 ms. We may estimate a mean survival time of (1.6 ± 0.3) ms when the He pressure was set to 420 mbar.

This is also in agreement with recent results obtained by Van Duppen et al. [21] who showed that the survival time of ions in a laser ion source was gradually decreasing with increasing beam intensity, from 20 ms for 10 enA of ^{3}He in the gas cell down to 3 ms with 1000 enA. This is of course of importance because the IGISOL technique could be applied under more extreme conditions, for example, with very high primary beam intensities.

3.4. Applications: EC / β^{+} decay study of $^{132}Nd \rightarrow {}^{132}Pr \rightarrow {}^{132}Ce$

The IGISOL technique, having no Z-selectivity, is quite suitable for ionizing very refractory elements and therefore for the study of neutron-deficient isotopes of rare-earth elements. As an example of the first results obtained with this new set-up, we present in Fig. 10 a β-gated γ spec-

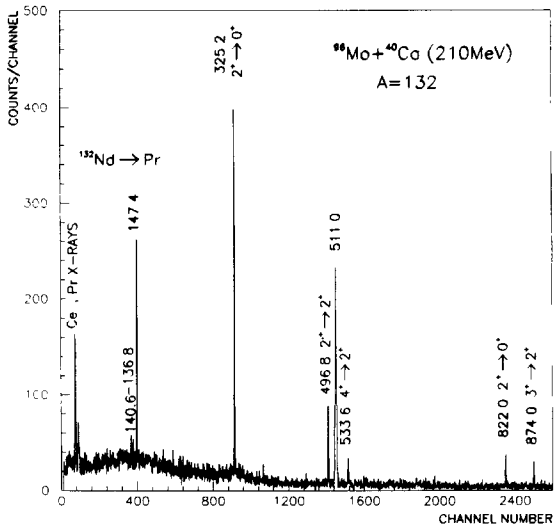

Fig. 10. β-gated γ spectrum measured at mass $A = 132$ with 100-s collection and counting times for about 10 hours. The reaction was $^{40}Ca^{11+}$ (210 MeV, $I = 500$ enA) bombarding a 2-mg/cm^2 ^{96}Mo target enriched to 97.8%.

trum of $A = 132$ activities produced in the $^{96}Mo + ^{40}Ca$ reaction.

Very scarce data were reported up to now on the EC/β^+ decay of ^{132}Nd, except for the half-life ($T_{1/2} = 105 \pm 10$ s) measured on X-rays by Bogdanov et al. [22] using the reaction $^{106}Cd + ^{32}S$ at 180-MeV bombarding energy. Low-energy levels populated in ^{132}Pr ($T_{1/2} = 1.6$ min) β-decay chain have been previously studied at SARA by using the He jet technique [23].

In Fig. 10 the first transitions of the ground-state and γ-bands in ^{132}Ce as well as the $2'^+ \rightarrow 0^+$ (822 keV) transition are seen. In this spectrum three new γ-ray transitions were observed and unambiguously assigned to ^{132}Nd. The half-life determined from the decay of these γ lines has an average value $T_{1/2} = (100 \pm 10)$ s in good agreement with ref. [22].

4. Conclusion

This new IGISOL chamber designed for the on-line mass separation of short-lived neutron-deficient nuclei synthesized in heavy-ion-induced fusion–evaporation reactions is based on the kinematic separation of beam particles and EVRs to reduce the plasma effect.

The absolute efficiency obtained in this work ($> 10^{-3}$) is comparable to the one achieved with a double chamber in fission reactions. The IGISOL technique has already proved to be a powerful tool for the study of short-lived (down to ms range) isotopes of refractory elements produced by charged particle induced fission on ^{238}U. Obviously by careful adjustments the technique has now reached a level which is promising for the identification and study of exotic nuclei produced in (HI, xn) reactions.

Recently the new SARA IGISOL system was successfully applied in our experiments on the observation of alpha-decay of the isotope ^{180}Tl produced in the $^{144}Sm + ^{40}Ca$ reaction. These results are reported elsewhere [24].

Acknowledgements

This work has been performed in the framework of the JINR Dubna–IN2P3 (CNRS) collaboration. We are much indebted to Yu.Ts. Oganessian for continuous support of this program. Our thanks are due to R.N. Sagaidak for numerous calculations of the reaction kinematics carried out in the course of the present work. We are grateful to J.P. Richaud, L. Vidal for target and window preparation. Z. Preibisz and F. Morel are acknowledged for their participation in the experiments and their help in data analysis.

References

[1] J. Ärje, J. Äystö, H. Hyvönen, P. Taskinen, V. Koponen, J. Honkanen, A. Hautojärvi and K. Vierinen, Phys. Rev. Lett. 54 (1985) 99.

[2] K. Morita, T. Inamura, T. Nomura, J. Tanaka, H. Miyatake, M. Fujioka, T. Shinozuka, M. Yoshii, H. Mama, K. Taguchi, K. Sueki, Y. Hatsukawa, K. Furuno and H. Kudo, Nucl. Instr. and Meth. B 26 (1987) 406.

[3] K. Deneffe, B. Brijs, E. Coenen, J. Gentens, M. Huyse, P. Van Duppen and D. Wouters, Nucl. Instr. and Meth. B 26 (1987) 399.

[4] P. Taskinen, H. Penttilä, J. Äystö, P. Dendooven, P. Jauho, A. Jokinen and M. Yoshii, Nucl. Instr. and Meth. A 281 (1989) 539.

[5] T. Nomura, J. Tanaka, M. Oyaizu, Y. Iwata, N. Ikeda, K. Valli, K. Morita, Y. Nagai, T. Toriyama, Y. Murakami, Y. Torii and S. Harada, Nucl. Instr. and Meth. A 269 (1988) 23.

[6] K. Morita, T. Nomura, A. Yoshida, T.T. Inamura, M. Koizumi, M. Fujioka, T. Shinozuka, H. Miyatake, K. Sueki, H. Kudo, Y. Nagai, K. Yoshimura, T. Toriyama and Y. Hatsukawa, EMIS-12 Int. Conf. on Electromagnetic Isotope Separators and Techniques Related to their Applications, Sept. 2–6, 1991 Sendai, Japan, Abstract D02, p. 20.

[7] G.D. Sprouse, J Das, T. Lauritsen, J Schecker, A. Berger, C.H. Holbrow, H.E. Mahnke and S.L. Rolston, Phys Rev. Lett. 63 (1989) 1463.

[8] A. Ewart and M. Kaplan, Phys. Rev. 162, (1967) 944.

[9] L. Handschug and H. Backe, Nucl. Instr. and Meth. 161 (1979) 117.

[10] J.S. Dionisio, Ch. Vieu, J.M. Lagrange, M. Pautrat, J. Vanhorenbeck and A. Passoja, Nucl. Instr. and Meth. A 282 (1989) 10.

[11] Yu.A. Lazarev, Yu.Ts. Oganessian, I.V. Shirokovsky, S.P. Tretyakova, V.K. Utyonkov and G.V Buklanov, Europhys. Lett. 4 (1987) 893;
6th Int. Conf. on Nuclei Far from Stability and 9th Int. Conf.

on Atomic Masses and Fundamental Constants, Bernkastel-Kues, Germany, eds. R. Neugart and A. Wöhr (IOP, Bristol, 1992) p. 739.
[12] R.N. Sagaidak, JINR preprint P7-89-551, Dubna (1981); Heavy Ion Physics, Scientific Report 1989–1990, JINR, E7-91-75, Dubna (1991) p. 125, and private communications.
[13] L.C. Northcliffe and R.F. Shilling, Nucl. Data Tables A 7 (1970) 233.
[14] TRIM-code, J.F. Ziegler, J.P. Biersack and U. Littmark, The Stopping and Range of Ions in Matter, Vol. 1, ed. J.F. Ziegler (Pergamon, New York, 1985).
[15] A. Astier, R. Béraud, A. Bouldjedri, R. Duffait, A. Emsallem, M. Meyer, S. Morier, P. Pangaud, N. Redon, D. Barnéoud, J. Blachot, J. Genevey, A. Gizon, R. Guglielmini, J. Inchaouh, G. Margotton, J.L. Vieux-Rochaz, J. Ärje, J. Äystö, P. Jauho, A. Jokinen, H. Penttilä, K. Eskola, M. Leino and J.B. Marquette, Nucl. Instr. and Meth. B 70 (1992) 233.
[16] C.N. Davids, Nucl. Instr. and Meth. B 70 (1992) 435.
[17] A. Iivonen, J. Kuhalainen, R. Saintola, K. Valli, T. Inamura, M. Koizumi, K. Morita and A Yoshida, Nucl. Instr. and Meth. B 70 (1992) 213.
[18] M.A. Biondi and S.C. Brown, Phys. Rev. 75 (1949) 1700.
[19] J.B. Natowitz and J.M. Alexander, Phys. Rev. 188 (1969) 1734
[20] J. Ärje, Ph.D. Thesis, Jyväskylä (1986).
[21] P. Van Duppen, N. Bijnens, M. Huyse, Y.A. Kudryavtsev, L. Vermeeren, Z N. Qamhieh, P.H. Thoen, E. Vandeweert and R.E. Silverans, Midsummer Workshop on Nuclear Physics, Jyväskylä, June 8–12, 1993 and to be published.
[22] D.D. Bogdanov, A.V. Demyanov, V.A. Karnaukhov, L.A. Petrov, A. Plohocki, V.G Subbotin and J. Voboril, Nucl. Phys. A 275 (1977) 229.
[23] D. Barnéoud, J. Blachot, J. Genevey, A. Gizon, R. Béraud, R. Duffait, A. Emsallem, M. Meyer, N. Redon and D. Rolando-Eugio, Z. Phys. A 330 (1988) 341.
[24] Yu.A. Lazarev, I.V. Shirokovsky, I.N. Izosimov, A. Emsallem, R. Béraud, A. Astier, Y. Le Coz, A. Gizon, J. Genevey and D. Barnéoud, to be published.